IJMMM International Journal of Minerals, Metallurgy and Materials 矿物冶金与材料学报（英文版）

Sandwich-like structure C/SiO_x@graphene anode material with high electrochemical performance for lithium ion batteries

Zhaolin Li, Yaozong Yang, Jie Wang, Zhao Yang, and Hailei Zhao

Cite this article as:
Zhaolin Li, Yaozong Yang, Jie Wang, Zhao Yang, and Hailei Zhao, Sandwich-like structure C/SiO_x@graphene anode material with high electrochemical performance for lithium ion batteries, *Int. J. Miner. Metall. Mater.*, 29(2022), No. 11, pp. 1947-1953. https://doi.org/10.1007/s12613-022-2526-0

Articles you may be interested in

Zhi-yuan Feng, Wen-jie Peng, Zhi-xing Wang, Hua-jun Guo, Xin-hai Li, Guo-chun Yan, and Jie-xi Wang, Review of silicon-based alloys for lithium-ion battery anodes, *Int. J. Miner. Metall. Mater.*, 28(2021), No. 10, pp. 1549-1564. https://doi.org/10.1007/s12613-021-2335-x

Li-fan Wang, Meng-meng Geng, Xia-nan Ding, Chen Fang, Yu Zhang, Shan-shan Shi, Yong Zheng, Kai Yang, Chun Zhan, and Xin-dong Wang, Research progress of the electrochemical impedance technique applied to the high-capacity lithium-ion battery, *Int. J. Miner. Metall. Mater.*, 28(2021), No. 4, pp. 538-552. https://doi.org/10.1007/s12613-020-2218-6

Qi Wang, Yue-yong Du, Yan-qing Lai, Fang-yang Liu, Liang-xing Jiang, and Ming Jia, Three-dimensional antimony sulfide anode with carbon nanotube interphase modified for lithium-ion batteries, *Int. J. Miner. Metall. Mater.*, 28(2021), No. 10, pp. 1629-1635. https://doi.org/10.1007/s12613-021-2249-7

Qiao-kun Du, Qing-xia Wu, Hong-xun Wang, Xiang-juan Meng, Ze-kai Ji, Shu Zhao, Wei-wei Zhu, Chuang Liu, Min Ling, and Cheng-du Liang, Carbon dot-modified silicon nanoparticles for lithium-ion batteries, *Int. J. Miner. Metall. Mater.*, 28(2021), No. 10, pp. 1603-1610. https://doi.org/10.1007/s12613-020-2247-1

Ying-jun Qiao, Huan Zhang, Yu-xin Hu, Wan-peng Li, Wen-jing Liu, Hui-ming Shang, Mei-zhen Qu, Gong-chang Peng, and Zheng-wei Xie, A chain-like compound of Si@CNT nanostructures and MOF-derived porous carbon as an anode for Li-ion batteries, *Int. J. Miner. Metall. Mater.*, 28(2021), No. 10, pp. 1611-1620. https://doi.org/10.1007/s12613-021-2266-6

Jun Yang, Yuan-hua Lin, Bing-shu Guo, Ming-shan Wang, Jun-chen Chen, Zhi-yuan Ma, Yun Huang, and Xing Li, Enhanced electrochemical performance of Si/C electrode through surface modification using SrF_2 particle, *Int. J. Miner. Metall. Mater.*, 28(2021), No. 10, pp. 1621-1628. https://doi.org/10.1007/s12613-021-2270-x

IJMMM WeChat

QQ author group

International Journal of Minerals, Metallurgy and Materials
Volume 29, Number 11, November 2022, Page 1947
https://doi.org/10.1007/s12613-022-2526-0

Sandwich-like structure C/SiO_x@graphene anode material with high electrochemical performance for lithium ion batteries

Zhaolin Li[1),*], *Yaozong Yang*[1),*], *Jie Wang*[1)], *Zhao Yang*[1)], *and Hailei Zhao*[1,2),✉]

1) School of Materials Science and Engineering, University of Science and Technology Beijing, Beijing 100083, China
2) Beijing Municipal Key Laboratory of New Energy Materials and Technologies, Beijing 100083, China
(Received: 11 June 2022; revised: 10 July 2022; accepted: 12 July 2022)

Abstract: Silicon suboxide (SiO_x, $0 < x < 2$) is recognized as one of the next-generation anode materials for high-energy-density lithium ion batteries (LIBs) due to its high theoretical specific capacity and abundant resource. However, the severe mechanical instability arising from large volume variation upon charge/discharge cycles frustrates its electrochemical performance. Here we propose a well-designed sandwich-like structure with sandwiched SiO_x nanoparticles between graphene sheets and amorphous carbon-coating layer so as to improve the structural stability of SiO_x anode materials during cycling. Graphene sheets and carbon layer together construct a three-dimensional conductive network around SiO_x particles, which not only improves the electrode reactions kinetics, but also homogenizes local current density and thus volume variation on SiO_x surface. Moreover, Si–O–C bonds between SiO_x and graphene endow the strong particle adhesion on graphene sheets, which prevents SiO_x peeling from graphene sheets. Owing to the synergetic effects of the structural advantages, the C/SiO_x@graphene material exhibits an excellent cyclic performance such as 890 mAh/g at 0.1 C rate and 73.7% capacity retention after 100 cycles. In addition, it also delivers superior rate capability with a capacity recovery of 886 mAh/g (93.7% recovery rate) after 35 cycles of ascending steps at current range of 0.1–5 C and finally back to 0.1 C. This study provides a novel strategy to improve the structural stability of high-capacity anode materials for lithium/sodium ion batteries.

Keywords: sandwich-like structure; silicon suboxide; electrochemical performance; anode; lithium-ion battery

1. Introduction

Silicon suboxide (SiO_x, $0 < x < 2$) is considered as one of the most attractive anode materials for high-energy-density lithium ion batteries (LIBs) because of its ultrahigh theoretical specific capacity (about 2600 mAh/g), low operating voltage (about 0.4 V vs. Li/Li^+), rich natural resource, and environmental benignity [1–3]. However, its huge volume variation upon lithium uptake and release (about 160vol%) easily leads to particle fractures, resulting in continual structural deformation and eventually capacity loss of SiO_x-based electrodes. In addition, the low intrinsic electric conductivity of Si seriously slows the electrode reaction kinetics and thereby reduces the capacity utilization. The two abovementioned drawbacks of SiO_x severely hinder its further practical application in next-generation high energy density LIBs.

Tremendous efforts have been devoted to improving the structural stability and cyclic performance of SiO_x-based materials. Nano-SiO_x and SiO_x–C materials are regarded as the most effective strategies to improve the electrochemical performance of SiO_x according to the previous reports [4–9]. Nanosized particle can efficaciously release the structural stress induced during lithiation/delithiation process, resulting in the good structure durability of SiO_x materials. However, the complex preparation and high manufacture cost of well-dispersed SiO_x nanoparticles hinder the practical applications. Similar to other high-capacity electrode materials [10–12], compositing SiO_x with carbonaceous materials is an effective and economic approach to improve the electrochemical performance of SiO_x materials owing to the high electronic conductivity and relatively low-cost of carbon. Nevertheless, the continuous structure deterioration of SiO_x causes the departure between SiO_x and carbon, resulting in the loss of electric contact and thus fast capacity degradation of SiO_x. In this case, the electrochemical performance of SiO_x–C composite materials is still not satisfied to the commercial application in LIBs. Therefore, it is of great urgency to develop an effective approach to achieve a high-performance SiO_x–C anode material so as to further boost the practical use of SiO_x-based anode materials in high-energy-density LIBs.

Herein, we successfully prepared a C/SiO_x@graphene material with a sandwich-like structure of C–SiO_x–graphene via a facile and effective alcoholysis process at ambient temperature. Nanosized SiO_x particles conformally distribute on graphene sheets, which is uniformly coated by amorphous carbon layers. Graphene sheets and amorphous carbon layer

*These authors contributed equally to this work.
✉ Corresponding author: Hailei Zhao E-mail: hlzhao@ustb.edu.cn

together construct a three-dimension (3D) electron transport network around SiO_x, which homogenizes the local current density and ensures the uniform occurrence of electrode reactions on SiO_x, thus resulting in the homogeneous volume variation and excellent structure stability of C/SiO_x@graphene material. Moreover, Si–O–C bonds between SiO_x and graphene guarantee the strong adhesion of SiO_x particles on graphene sheets, which prevents the peeling and loss of electric contact of SiO_x particles, thus ensuring the excellent structural durability of C/SiO_x@graphene material during cycling. Owing to the structural advantages, the C/SiO_x@graphene material presents an excellent cyclic performance (890 mAh/g after 100 cycles at current density of 0.1 C with capacity retention of 73.7%) and superior rate capability (~400 mAh/g at 5 C rate). This work provides a valuable exploration for development of high-energy-density lithium-ion batteries.

2. Experimental

2.1. Material synthesis

2.1.1. Preparation of SiO_2@reduced graphene oxide (rGO) and SiO_2–rGO

Graphene oxide (GO) was prepared by a modified Hummer's method using natural graphite flasks (Alfa Aesar, Britain) as raw material. GO powder was calcinated at 700°C under Ar atmosphere to get reduced graphene oxide (rGO) without any oxygen-contained functional groups (Fig. S1). SiO_2@rGO material was synthesized via a facile alcoholysis approach at ambient temperature. Typically, 300 mg GO powder was dissolved into 15 mL ethylene glycol (EG, $Eg(OH)_2$ in Fig. 1(a)) with stirred for 2 h. Then, 5 mL silicon tetrachloride ($SiCl_4$) was dropwise added into the GO solution under continuous stirring followed by 4 h stirring at room temperature. The obtained brown paste was put into oven to remove solvent at the temperature of 120°C, which was then calcinated at 500°C under flowing Ar atmosphere to obtain SiO_2@rGO precursor material. Simultaneously, SiO_2–rGO material was prepared with rGO powder instead of GO via the same approach.

2.1.2. Preparation of SiO_x@rGO and SiO_x–rGO

SiO_2@rGO precursor powder was mixed with NaCl and Mg under the mass ratio of 1:10:0.9 by hand-grinding in agate mortar. Then the solid mixture was loaded into SS 316 Swagelok-type reactors in an argon-filled glovebox (<0.1 ppm H_2O, <0.1 ppm O_2), followed by heating in a tube furnace at 650°C for 4 h under an Ar atmosphere. After cooling down to ambient temperature, the obtained powder was successively washed with 1 M HCl solution and deionic water and then vacuum-dried at 80°C to get SiO_x@rGO precursor material. Meanwhile, SiO_x–rGO material was prepared via the same magnesiothermic reduction process.

2.1.3. Preparation of C/SiO_x@rGO

Sandwich-like structure C/SiO_x@rGO material was synthesized by a chemical vapor deposition method. First, 1 g of SiO_x@rGO powder was placed in a tube furnace, which was heated to 700°C at a temperature ramping rate of 5°C/min under an Ar gas flow. Then the gas flow was switched to acetylene/Ar mixture gas (10vol% diluted in Ar) for 30 min, when the temperature reached 700°C. Finally, the C/SiO_x@rGO was collected after the furnace cooling down.

2.2. Physical characterization

The particle morphology was observed by the field emission scanning electron microscopy (FESEM, Tecnai,

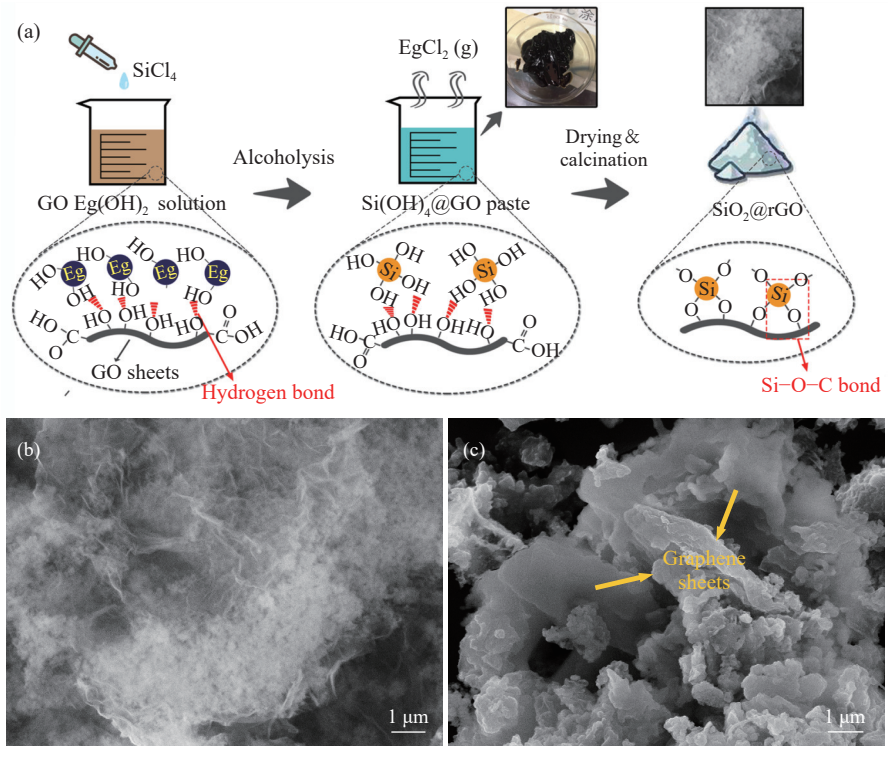

Fig. 1. (a) Schematic illustration in preparation process of SiO_2@rGO material and FESEM images of (b) SiO_2@rGO and (c) SiO_2–rGO materials.

SUPRA55, Germany) and transmission electron microscopy (TEM, FEI Tecnai, F20, USA). Phase structure was detected by the Raman spectroscopy (HORIBA Scientific LabRAM HR Evolution, Japan) and the X-ray diffraction (XRD, RIGAKU, Japan, D/max-A, Cu K_α, λ = 0.15406 nm). Fourier transform infrared spectroscopy (FTIR, Thermo Scientific Nicolet iS20, USA) was conducted to analyze the bond structures. X-ray photoelectron spectroscopy (XPS, PerkinElmer PHI 5000C ESCA system, USA) using the Mg K_α radiation was performed to characterize the electron binding energies.

2.3. Electrochemical evaluation

The working electrodes were prepared with an active materials/carboxymethylcellulose (CMC)/acetylene mass ratio of 70:15:15. The prepared electrodes were assembled in 2032-type coin cells with lithium foil as counter electrode, porous polypropylene film (Celgard 2400) as separator, and 1 M $LiPF_6$ in the mixture of ethylene carbonate (EC), diethyl carbonate (DEC), and dimethyl carbonate (DMC) with the volume ratio of 1:1:1 as electrolyte. The mass loading of the prepared electrodes was 1.5 mg/cm^2. Galvanostatic discharge–charge tests were conducted on LAND CT2001A system (Wuhan, China) within the voltage range of 0.01–1.5 V vs. Li/Li^+.

3. Results and discussion

The schematic illustration in preparation process of SiO_x@rGO material is presented in Fig. 1(a). GO was beforehand dissolved in EG to form the GO $Eg(OH)_2$ solution, in which EG molecules combined with GO sheets via hydrogen bonds. Then $SiCl_4$ was dropwise added under continuous stirring, and meanwhile the alcoholysis reaction (Eq. (1)) with EG anchoring on GO sheets gradually occurred with heat release and pungent smell (dichloroethane, $EgCl_2$).

$$SiCl_4 + 3HOCH_2 - CH_2OH \rightarrow Si(OH)_4 + 2ClCH_2 - CH_2OH\,(l) + ClCH_2 - CH_2Cl\,(g) \quad (1)$$

After 4 h stirring, the *in-situ* formed $Si(OH)_4$ combined with GO sheets via hydrogen bonds, forming the $Si(OH)_4$@GO composite. Meanwhile, with the proceeding of alcoholysis reaction, the terreous solution turned to a dark-brown paste as shown in the inset Fig. 1(a). Subsequently, the $Si(OH)_4$@GO paste successively underwent a drying and calcination process, during which the dehydration reaction took place with the generation of Si–O–C bonds between SiO_2 and GO sheets. The FESEM image of prepared SiO_2@rGO shows that SiO_2 nanoparticles (NPs) conformally distribute on graphene sheets (Fig. 1(b)), which is attributed to the bi-functional EG. On one hand, the EG serves as a reactant in alcoholysis reaction (Eq. (1)) with $SiCl_4$ to form SiO_2 NPs. On the other hand, the GO-anchored EG molecules act as templates to induce the formation of conformally-coating SiO_2 NPs on GO sheets. On the contrary, the SiO_2–rGO material synthesized with rGO sheets without any functional groups exhibits obvious particle aggregations with severely stacked graphene sheets and aggregated SiO_2 NPs (Fig. 1(c)). Notably, the stacked graphene sheets are bared without any loaded SiO_2 NPs, indicating the critical role of bi-functional EG on uniform distribution of SiO_2 NPs on graphene sheets.

The SiO_x@rGO was prepared via a modified magnesiothermic reduction process according to the Eq. (2).

$$SiO_2 + (2-x)Mg \rightarrow SiO_x + (2-x)MgO \quad (2)$$

The FESEM image of SiO_x@rGO material shows that it still maintains the laminar structure even after the exothermal magnesiothermic reduction (Fig. 2(a)). Moreover, the magnified image clearly presents the conformal distribution of SiO_x NPs on graphene sheets (Fig. 2(b)), which is similar to that of SiO_2@rGO (Fig. 1(b)). The excellent structural stability is attributed to the Si–O–C bonds existing between SiO_x and rGO, resulting in the strong adhesion of SiO_x particles on graphene sheets. After the carbon coating, the laminar structure in C/SiO_x@rGO material is still preserved (Fig. 2(c)), which is in favor of the electrolyte penetration and rate capability. The larger particle size further indicates the carbon coating layer on SiO_x particles (Fig. 2(d)). Moreover, the TEM image of C/SiO_x@rGO material shows that SiO_x nanoparticles with particle diameter of ~50 nm uniformly distribute on rGO sheets (Fig. 2(e)), which is agreed to the FESEM results. The high-resolution TEM image clearly presents a single SiO_x particle with an outer amorphous carbon coating layer (thickness of ~2 nm) on surface, suggesting the C–SiO_x–rGO sandwich-like structure (Fig. 2(f)).

In order to elucidate the chemical structures, Raman, FTIR, and XPS measurements were conducted and the related results are presented in Fig. 3. The Raman peaks of both SiO_x–rGO and SiO_x@rGO composites located at ~490 and

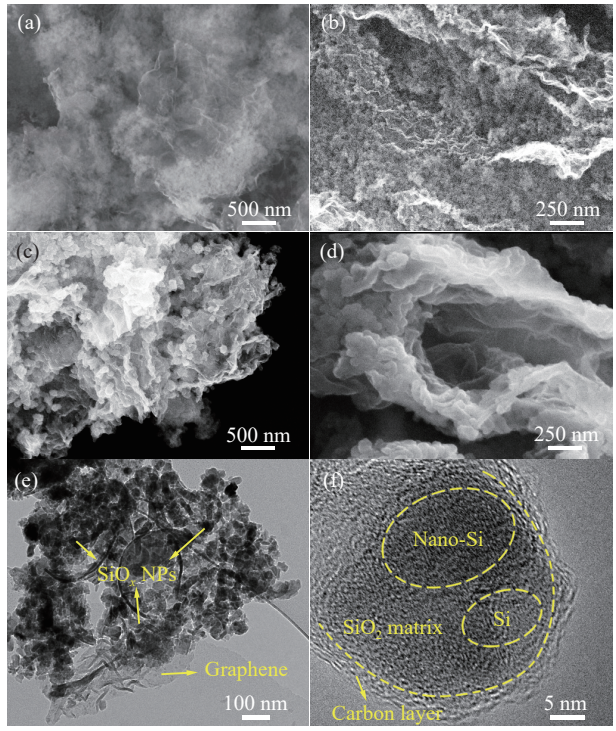

Fig. 2. FESEM images of (a, b) SiO_x@rGO and (c, d) C/SiO_x@rGO materials and (e, f) TEM images of C/SiO_x@rGO material.

908 cm^{-1} are in excellent accordance with Si band (Fig. 3(a)) [13], which is agreed with the XRD results (Fig. S2). In addition, the peak centered at 417 cm^{-1} is assigned to the O–Si–O linkage, while the peaks situated at ~585, 685, and 785 cm^{-1} are associated with the Si–O–Si bonds [14–16]. More importantly, a significant blue-shifting Si–Si bond in the Raman spectrum of SiO_x@rGO can be clearly observed, revealing the stronger Si–Si backbone due to the lower oxygen content in SiO_x. Meanwhile, the lower peak intensity of O–Si–O and Si–O–Si bonds further demonstrate the lower oxygen content in SiO_x of SiO_x@rGO, which is attributed to a more sufficient magnesiothermic reduction arising from the full contact between Mg vapor and conformally-distributed SiO_2 NPs on graphene sheets. The three bands at 1105, 883, and 471 cm^{-1} in the FTIR spectrum of SiO_x@rGO material are assignable to Si–O–Si asymmetric stretching, symmetric stretching, and bending vibrations, respectively (Fig. 3(b)) [17]. It is noteworthy that the absorption peak centered at 1070 cm^{-1} is related to Si–O–C bond [18], which is in accordance with the alcoholysis reaction mechanism proposed in Fig. 1(a).

Fig. 3(c) and (d) presents the Si 2p XPS spectra of SiO_x@rGO and SiO_x–rGO materials, respectively. The two main broad peaks in the spectrum of SiO_x@rGO composite can be fitted into four small peaks centered at 103.6, 102.3, 100.5, and 99.5 eV, which are associated with Si–O, Si–O–C,

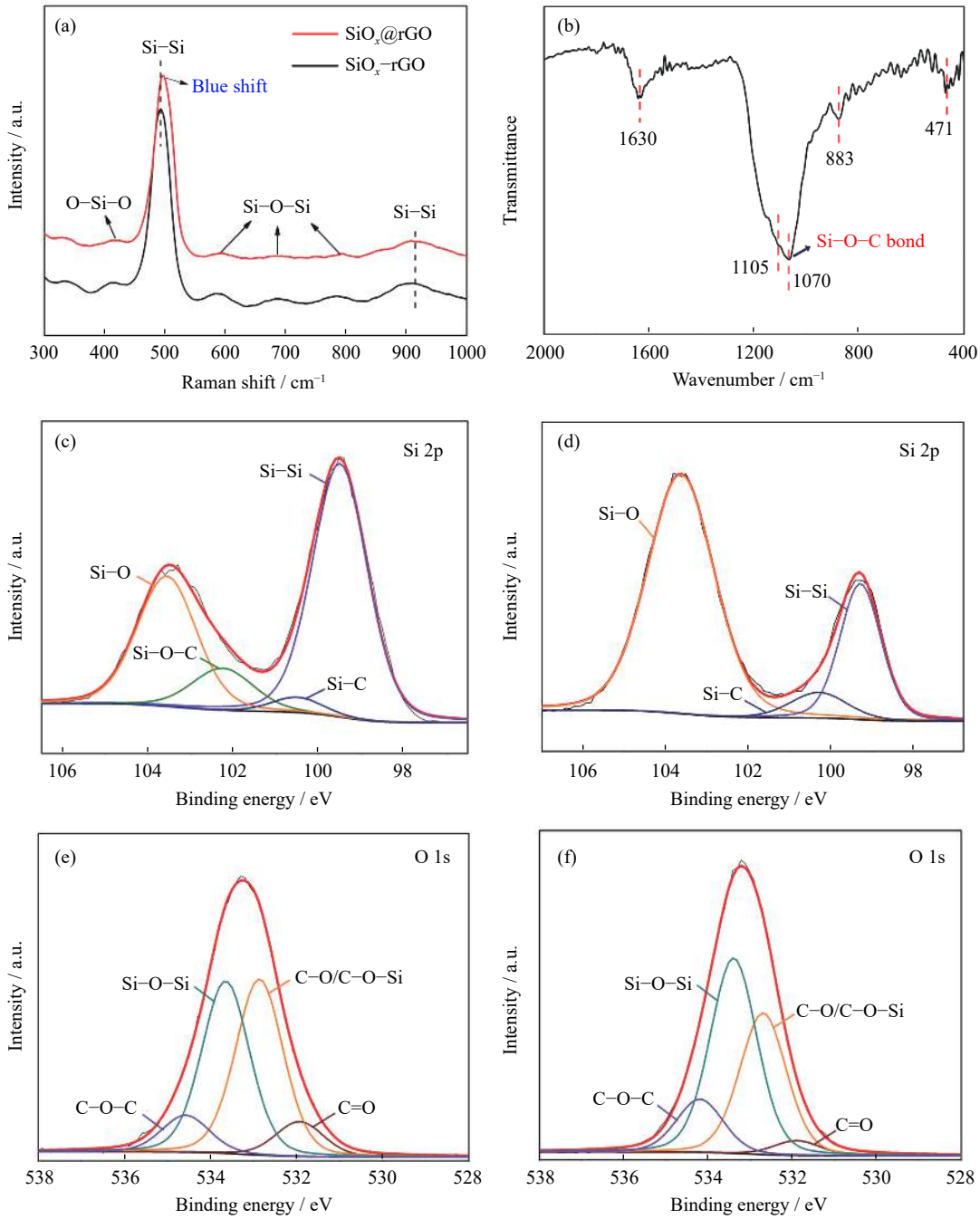

Fig. 3. (a) Raman spectra of SiO_x@rGO and SiO_x–rGO materials, (b) FTIR spectrum of SiO_x@rGO composite, and high-resolution Si 2p and O 1s XPS spectra of (c, e) SiO_x@rGO and (d, f) SiO_x–rGO materials.

Si–C, and Si–Si bonds, respectively (Fig. 3(c)) [19–22]. With respect to the Si 2p spectrum of SiO$_x$–rGO, it can be fitted into the small peaks of Si–O, Si–C, and Si–Si bonds (Fig. 3(d)). Intuitively, the peak intensity of Si–Si bond is much higher than that of Si–O bond in SiO$_x$@rGO and the related average valence state of Si is estimated to be +2.6 (x = 1.3 in SiO$_x$) based on the respective area of Si–Si and Si–O peaks. On the contrary, the peak intensity of Si–Si bond is much lower than that of Si–O bond in SiO$_x$–rGO spectrum, corresponding to a higher average valence state of Si element (+3). The lower oxygen content is owing to the more sufficient magnesiothermic reduction of conformally-coating SiO$_2$ NPs on graphene sheets in SiO$_2$@rGO precursor, which is agreed with the blue shift in Raman result (Fig. 3(a)). Moreover, the Si–O–C peak centered at 102.2 eV in Si 2p spectrum (Fig. 3(c)), as well as the stronger peak of C–O/C–O–Si bonds centered at 532.8 eV in O 1s spectrum (Fig. 3(e)) [23], further indicates the existence of Si–O–C bridging bonds between SiO$_x$ NPs and graphene sheets in SiO$_x$@rGO material. In addition, the peak situated at ~532 cm^{-1} is related to carbonyl groups originated from the residual oxygen-contained functional group on rGO [24]. Surprisingly, both the Si 2p XPS spectra of SiO$_x$@rGO and SiO$_x$–rGO show the weak peaks of Si–C bond at ~100.5 eV, which is associated with silicon carbide (SiC). This is consistent with the XRD result shown in the supplementary information (Fig. S2). The chemical reaction between ultrafine SiO$_2$ particles and carbon carbonized from ethylene chlorohydrin (formed according to Eq. (1)) may be accounted for the formation of SiC.

The electrochemical measurements were performed based on a half-cell configuration using metallic lithium foils as counter electrodes. The galvanostatic charge/discharge profiles of SiO$_x$@rGO electrode present an initial specific charge capacity of 1278 mAh/g and an initial Coulombic efficiency (ICE) of 74.8%, which are both higher than those of the SiO$_x$–rGO electrode (1104 mAh/g and 67.9%). The higher electrochemical performance of SiO$_x$@rGO electrode is beneficial from the more sufficient magnesiothermic reduction and therefore lower oxygen content in SiO$_x$ (Fig. 4(a)). With respect to the sandwich-like structure C/SiO$_x$@rGO material, it delivers a reversible specific capacity of 890 mAh/g and an ICE of 47%. The relatively low ICE is ascribed to the amorphous carbon with pretty high irreversible capacity which can be evidenced by the much longer slope in the charge/discharge profiles of C/SiO$_x$@rGO electrode. This low ICE can be addressed by employing prelithiation techniques in the future study [25–27]. Subsequently, the electrodes undergo a repeated galvanostatic cycling at the current density of 0.1 C within the voltage range of 0.01–1.5 V (Fig. 4(b)). Compared to SiO$_x$–rGO, the SiO$_x$@rGO electrode presents a relatively higher cyclic performance which is attributed to the Si–O–C bonds and thereby strong adhesion of SiO$_x$ NPs on graphene sheets. As for the C/SiO$_x$@rGO, it delivered an excellent cyclic performance with a high capacity retention (73.7%) and Coulombic efficiencies in the repeated cycles, suggesting a physically and chemically stable solid electrolyte interface (SEI) film in C/SiO$_x$@rGO electrode, which is owing to the well-designed sandwich-like C–SiO$_x$–graphene structure.

Rate performance were tested at various current densities from 0.1 to 5 C (Fig. 4(c)). The C/SiO$_x$@rGO electrode presents the reversible specific capacity of 946.7, 896.5, 830.1, 725.6, 596.8, 512.0, and 395.9 mAh/g at the current densities of 0.1, 0.2, 0.5, 1, 2, 3, and 5 C, respectively. With

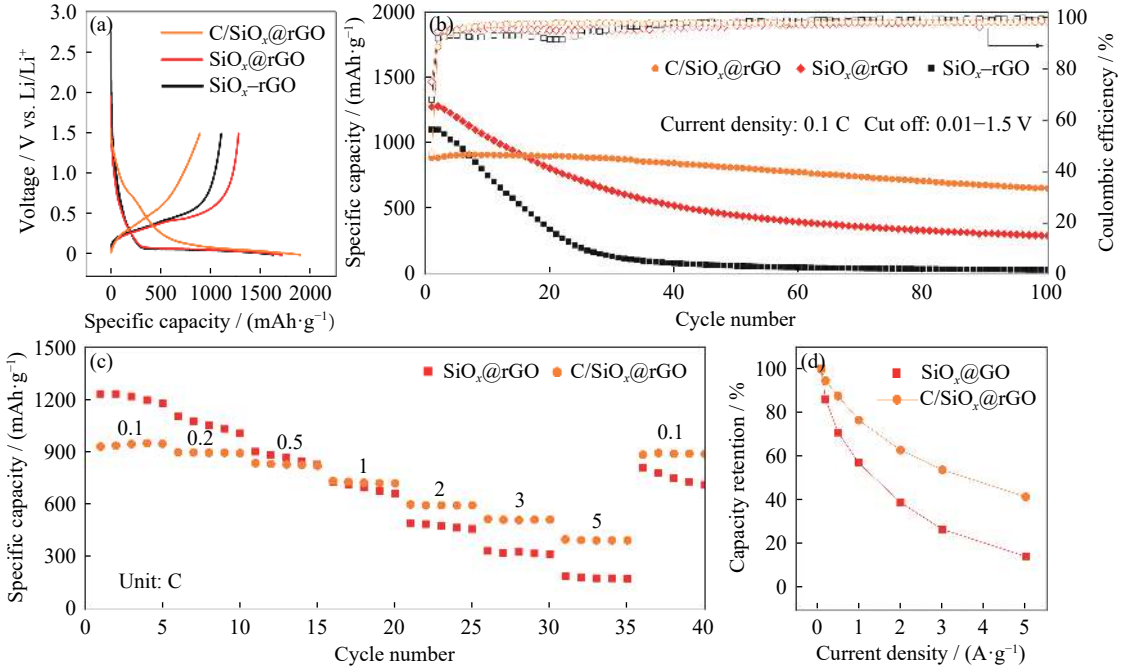

Fig. 4. (a) Galvanostatic charge–discharge curves and (b) cyclic performance of C/SiO$_x$@rGO, SiO$_x$@rGO, and SiO$_x$–rGO electrodes at the current density of 0.1 C (1 C = 1 A/g); (c) rate performance and (d) the related capacity retention of C/SiO$_x$@rGO and SiO$_x$@rGO electrodes.

respect to the SiO_x@rGO, it delivers a poor rate capability with a fast capacity decrease from 0.1 to 5 C due to the direct exposure of SiO_x NPs to electrolyte. The related capacity retentions, calculated based on the capacity of the 3rd cycle at each current rate, are summarized in Fig. 4(d). Obviously, the C/SiO_x@rGO electrode delivers a higher capacity retention than SiO_x@rGO at each current rate, indicating a superior rate performance. In addition, the differential capacity versus potential (dQ/dV) curves at different current densities show that the anodic peaks of C/SiO_x@rGO electrode present lower polarization than those of SiO_x@rGO electrode with the increase of current rate (Fig. S3(a) and (b)). Moreover, the lithium ion diffusion coefficient is calculated to be 1.4×10^{-12} cm^2/s according to the cyclic voltammetry (CV) curves at various scan rates (Fig. S3(c) and (d), detailed calculation seen in supplementary information) [28–29], which is much higher than that of pure SiO_x (~10^{-14} cm^2/s), suggesting a fast electrode reaction kinetics of C/SiO_x@rGO material. When switching back to 0.1 from 5 C, the C/SiO_x@rGO electrode presents a specific capacity of 886.3 mAh/g accompanying with a capacity recovery rate of 93.7%, and the capacity is well-maintained in the following cycles, revealing a robust structure of C/SiO_x@rGO material even after ultra-fast charging/discharging process. The comparison of electrochemical properties suggests the high-level performance of C/SiO_x@rGO material among the previously-reported SiO_x–graphene composites (Table S1).

Based on the above discussions, the remarkable electrochemical performance in terms of excellent cyclic performance and superior rate capability is attributed to the well-elaborated sandwich-like structure in C/SiO_x@rGO material. A schematic illustration of the structural evolution during lithiation/delithiation process is presented in order to intuitively understand the critical role of sandwich-like structure on electrochemical performance (Fig. 5). The structural advantages in C/SiO_x@rGO material can be summarized as the following three aspects. First, the ultrafine SiO_x particles, achieved by a facile and controllable alcoholysis process, can effectively resist the inner structural stress induced by large volume variation of SiO_x, thus well-maintaining the structural integrity during lithiation and delithiation processes. Second, graphene sheets and amorphous carbon layer together construct a 3D conductive network for fast electron movement around SiO_x NPs, which effectively homogenizes local current density and electrode reactions on SiO_x, resulting in uniform volume variation and excellent structural durability of SiO_x during the repeated cycles. Third, Si–O–C bonds between SiO_x NPs and graphene sheets can strengthen the particle adhesion on graphene matrix, which prevents the peeling of SiO_x NPs from graphene sheets and therefore structural deterioration. Owing to the synergetic effects of structural merits, the sandwich-like C/SiO_x@rGO material shows a remarkable electrochemical performance in terms of excellent cyclic performance and rate capability.

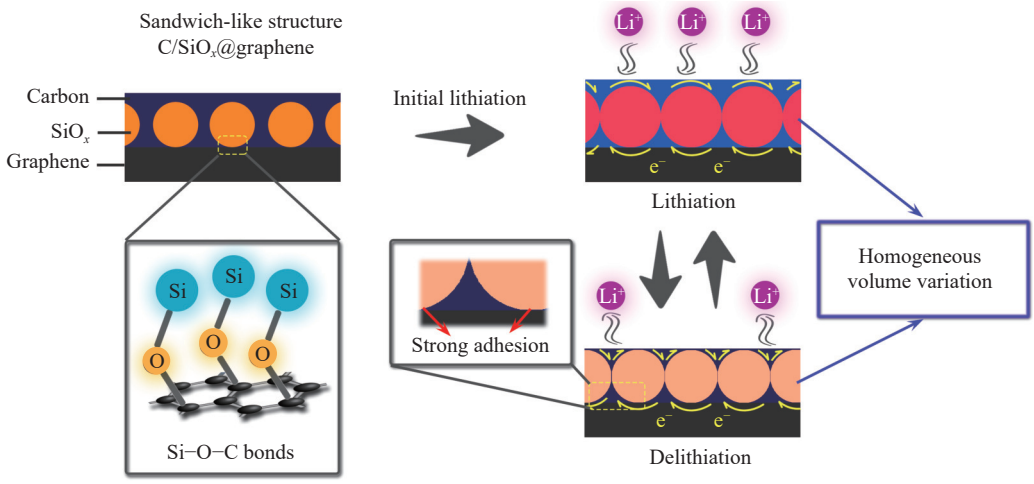

Fig. 5. Schematic illustration of the sandwich-like structure and its functions on lithiation/delithiation process of C/SiO_x@rGO material.

4. Conclusion

Herein, we successfully fabricated a sandwich-like structure C/SiO_x@rGO material via a facile and controllable alcoholysis process. In this well-engineered structure, a 3D highly-conductive network constructed by graphene sheets and amorphous carbon layer not only improves the electrode reaction kinetics of SiO_x, but also ensures the uniform local current density and electrode reactions on surface of SiO_x. Moreover, Si–O–C bonds existing between SiO_x and graphene strengthen the particle adhesion on graphene sheets, enabling the outstanding structural integrity during charge/discharge process. Benefiting from the above structural merits, the C/SiO_x@rGO material exhibits a remarkable electrochemical performance in terms of excellent cyclic performance and superior rate capability. The C/SiO_x@rGO electrode delivers a reversible specific capacity of 890 mAh/g and a high capacity retention of 73.7% after 100 cycles at the current density of 0.1 C. In addition, a capacity of ~400 mAh/g at 5 C, as well as a nearly full capacity recovery when switching back to 0.1 C is achieved. The elaborate structural design sheds light on the future improvement of

high-capacity electrode materials for lithium/sodium ion batteries.

Acknowledgements

This work was financially supported by the National Natural Science Foundation of China (Nos. 52102205 and U1637202) and the Fundamental Research Funds for the Central Universities (No. FRF-TP-20-048A1).

Conflict of Interest

The authors declare that they have no known competing financial interests or personal relationships that could have appeared to influence the work reported in this paper.

Supplementary Information

The online version contains supplementary material available at https://doi.org/10.1007/s12613-022-2526-0.

References

[1] H.Y. Li, H.D. Li, Z.W. Yang, *et al*., SiO_x anode: From fundamental mechanism toward industrial application, *Small*, 17(2021), No. 51, art. No. 2102641.

[2] L. Sun, Y.X. Liu, J. Wu, *et al*., A review on recent advances for boosting initial Coulombic efficiency of silicon anodic lithium ion batteries, *Small*, 18(2022), No. 5, art. No. 2102894.

[3] T. Chen, J. Wu, Q.L. Zhang, and X. Su, Recent advancement of SiO_x based anodes for lithium-ion batteries, *J. Power Sources*, 363(2017), p. 126.

[4] J.Y. Zhang, C.Q. Zhang, Z. Liu, *et al*., High-performance ball-milled SiO_x anodes for lithium ion batteries, *J. Power Sources*, 339(2017), p. 86.

[5] J.G. Guo, W. Zhai, Q. Sun, *et al*., Facilely tunable core–shell Si@SiO_x nanostructures prepared in aqueous solution for lithium ion battery anode, *Electrochim. Acta*, 342(2020), art. No. 136068.

[6] J. Peng, J. Luo, W.W. Li, *et al*., Insight into the performance of the mesoporous structure SiO_x nanoparticles anchored on carbon fibers as anode material of lithium-ion batteries, *J. Electroanal. Chem.*, 880(2021), art. No. 114798.

[7] Q. Xu, J.K. Sun, Y.X. Yin, and Y.G. Guo, Facile synthesis of blocky SiO_x/C with graphite-like structure for high-performance lithium-ion battery anodes, *Adv. Funct. Mater.*, 28(2018), No. 8, art. No. 1705235.

[8] Z.H. Liu, D.D. Guan, Q. Yu, *et al*., Monodisperse and homogeneous SiO_x/C microspheres: A promising high-capacity and durable anode material for lithium-ion batteries, *Energy Storage Mater.*, 13(2018), p. 112.

[9] W.L. Guo, X. Yan, F. Hou, *et al*., Flexible and free-standing SiO_x/CNT composite films for high capacity and durable lithium ion batteries, *Carbon*, 152(2019), p. 888.

[10] M.R. Wu, M.Y. Gao, S.Y. Zhang, *et al*., High-performance lithium–sulfur battery based on porous N-rich g-C_3N_4 nanotubes via a self-template method, *Int. J. Miner. Metall. Mater.*, 28(2021), No. 10, p. 1656.

[11] Y.R. Wang, L. Zhang, X.H. Gao, L.Y. Mao, Y. Hu, and X.W. Lou, One-pot magnetic field induced formation of Fe_3O_4/C composite microrods with enhanced lithium storage capability, *Small*, 10(2014), No. 14, p. 2815.

[12] D.L. Cheng, L.C. Yang, R.Z. Hu, *et al*., Sn–C and Se–C co-bonding SnSe/few-layered graphene micro–nano structure: Route to a densely compacted and durable anode for lithium/sodium-ion batteries, *ACS Appl. Mater. Interfaces*, 11(2019), No. 40, p. 36685.

[13] G.Q. Wang, Z.S. Wen, Y.E. Yang, *et al*., Ultra-long life Si@rGO/g-C_3N_4 with a multiply synergetic effect as an anode material for lithium-ion batteries, *J. Mater. Chem. A*, 6(2018), No. 17, p. 7557.

[14] V.D. Khavryuchenko, O.V. Khavryuchenko, and V.V. Lisnyak, Quantum chemical insight on vibration spectra of silica systems, *Mol. Simul.*, 33(2007), No. 6, p. 531.

[15] Y.F. Chen, F.F. Lai, and J.L. Li, Effect of B_2O_3 on structure of glassy F-free CaO–SiO_2–B_2O_3 systems by ^{29}Si MAS NMR and Raman spectroscopy, *JOM*, 72(2020), No. 3, p. 1414.

[16] A. Prasath, A.S. Sharma, and P. Elumalai, Nanostructured SiO_2@NiO heterostructure derived from laboratory glass waste as anode material for lithium-ion battery, *Ionics*, 25(2019), No. 3, p. 1015.

[17] Z.L. Li, H.L. Zhao, P.P. Lv, *et al*., Watermelon-like structured SiO_x–TiO_2@C nanocomposite as a high-performance lithium-ion battery anode, *Adv. Funct. Mater.*, 28(2018), No. 31, art. No. 1605711.

[18] F. Azimov, I. Markova, V. Stefanova, and K. Sharipov, Synthesis and characterization of SBA-15 and Ti-SBA-15 nanoporous materials for DME catalysts, *J. Univ. Chem. Technol. Metall.*, 47(2012), No. 3, p. 333.

[19] D.S. Wang, M.X. Gao, H.G. Pan, J.H. Wang, and Y.F. Liu, High performance amorphous-Si@SiO_x/C composite anode materials for Li-ion batteries derived from ball-milling and *in situ* carbonization, *J. Power Sources*, 256(2014), p. 190.

[20] F.F. Wang, S. Lin, X.S. Lu, R.Y. Hong, and H.Y. Liu, Polydopamine carbon-coated stable silicon/graphene/CNT composite as anode for lithium ion batteries, *Electrochim. Acta*, 404(2022), art. No. 139708.

[21] Y.D. Cao, S. Hans, J. Liese, *et al*., Si$(CO)_y$ negative electrodes for Li-ion batteries, *Chem. Mater.*, 33(2021), No. 18, p. 7386.

[22] M.Y. Gao, Z.H. Tang, M.R. Wu, *et al*., Self-supporting N, P doped Si/CNTs/CNFs composites with fiber network for high-performance lithium-ion batteries, *J. Alloys Compd.*, 857(2021), art. No. 157554.

[23] B. Ramezanzadeh, A. Ahmadi, and M. Mahdavian, Enhancement of the corrosion protection performance and cathodic delamination resistance of epoxy coating through treatment of steel substrate by a novel nanometric sol–gel based silane composite film filled with functionalized graphene oxide nanosheets, *Corros. Sci.*, 109(2016), p. 182.

[24] H.M. Xie, J.H. Dai, and D. Zhou, Tribological behaviors of graphene oxide partly substituted with nano-SiO_2 as lubricant additives in water for magnesium alloy/steel interfaces, *Int. J. Miner. Metall. Mater.*, 29(2022), No. 7, p. 1425.

[25] H. Zhao, Z.H. Wang, P. Lu, *et al*., Toward practical application of functional conductive polymer binder for a high-energy lithium-ion battery design, *Nano Lett.*, 14(2014), No. 11, p. 6704.

[26] J. Zhao, Z.D. Lu, N. Liu, H.W. Lee, M.T. McDowell, and Y. Cui, Dry-air-stable lithium silicide–lithium oxide core–shell nanoparticles as high-capacity prelithiation reagents, *Nat. Commun.*, 5(2014), No. 1, art. No. 5088.

[27] Z.Y. Cao, P.Y. Xu, H.W. Zhai, *et al*., Ambient-air stable lithiated anode for rechargeable Li-ion batteries with high energy density, *Nano Lett.*, 16(2016), No. 11, p. 7235.

[28] M.T. Duan, M.R. Wu, K. Xue, *et al*., Preparation of CoO/SnO_2@NC/S composite as high-stability cathode material for lithium–sulfur batteries, *Int. J. Miner. Metall. Mater.*, 28(2021), No. 10, p. 1647.

[29] L.J. Fu, H. Liu, H.P. Zhang, *et al*., Novel TiO_2/C nanocomposites for anode materials of lithium ion batteries, *J. Power Sources*, 159(2006), No. 1, p. 219.